Myeesha Mostafa, Mohammad Jellur Rahman* and Shamima Choudhury

Enhanced dielectric properties of $BaTiO_3$ ceramics with cerium doping, manganese doping and Ce-Mn co-doping

https://doi.org/10.1515/secm-2017-0177
Received May 20, 2017; accepted August 31, 2018; previously published online November 14, 2018

Abstract: $Ba_{1-x}Ce_xTi_{1-y}Mn_yO_3$ (where x and y varies from 0.00 to 0.03) ceramic samples are synthesized by conventional solid state reaction technique. The samples are sintered at 1473 K for 4 h. The grain size is observed to increase with increasing dopant and co-dopant concentration. The X-ray diffraction confirmed the cubic phase of these $BaTiO_3$-based ceramics with a small amount of secondary phase. The current density shows a nearly linear relationship with voltage, and the AC resistivity of the samples is observed to decrease with increasing frequency and doping concentration. The dielectric constant and dielectric loss were observed to decrease with frequency in the lower frequency range (0.2–10 kHz), but remained almost the same at the high-frequency region (>10 kHz). Though Ce-doped samples shows better dielectric properties than Mn-doped samples, the Ce-Mn co-doped samples, having improved their dielectric properties, can be used to fabricate different optoelectric devices.

Keywords: dielectric properties; grain size; resistivity; SEM; solid state reaction; XRD.

1 Introduction

Barium titanate ($BaTiO_3$) is a ferroelectric ceramics, which has been used for many years because of its enhanced dielectric properties [1]. It exists mainly in the tetragonal symmetry and holds a dielectric constant 100 times larger than that of other insulators [2, 3], high stability, and low leakage current and electro-optic coefficient [2]. Because of its simple structure, $BaTiO_3$ can react easily with other oxides to form solid solutions and, therefore, is useful for manufacturing various electronic components [3]. Owing to extremely high dielectric constant and low dielectric loss [1], $BaTiO_3$ doped with other rare earth elements was used to fabricate multilayer capacitors (MLCs) of electro-optic devices, semiconductors, PTC thermistors, and piezoelectric devices [1–4].

$BaTiO_3$ is a member of the perovskite family having the general form ABO_3 [1], where A is a monovalent, divalent, or trivalent metal, and B is a pentavalent, tetravalent, or trivalent element, respectively. $BaTiO_3$ can be doped with various types of dopants in order to improve its performance, to control the grain boundaries and also the electrical properties [3]. It was observed that the grain growth during the sintering of $BaTiO_3$, and the types and concentration of the additives in it, play important roles on its dielectric properties [3, 5, 6]. Depending on the valency and the types of substituting ions, it is possible to dope $BaTiO_3$ both at the A and B sites [7]. It can be doped with trivalent ions such as cerium (Ce), lanthanum, yttrium, and antimony on Ba-ion sites or with pentavalent ions like niobium, antimony, and tantalum on Ti-ion sites [8].

Ce is the most prolific rare earth element, which exists in both 4+ and 3+ oxidation states and can be substituted on both sites of $BaTiO_3$. When $BaTiO_3$ and CeO_2 are sintered in the presence of air with an additional amount of TiO_2, Ce is incorporated as a donor at the Ba-ion sites of $BaTiO_3$ [9]. On the other hand, when sintering is operated in $BaTiO_3$ and CeO_2 with excess amount of BaO, Ce is incorporated at the Ti sites [9]. In some research, it was observed that $BaTiO_3$ highly doped with Ce^{3+}, showing propitious dielectric properties such as high permittivity and high endurance [10]. It was also reported that the addition of Ce causes the increase in grain size of $BaTiO_3$ with sharp grain boundaries and a decrease in lattice parameter, a [2]. Therefore Ce doping can cause an improvement in the various properties of $BaTiO_3$.

Manganese (Mn) can exist in Mn^{2+}, Mn^{3+}, and Mn^{4+} states depending on the oxygen partial pressure and acts as an acceptor during the substitution in the B sites of the ABO_3 type materials [11]. When Mn^{4+} substitutes the Ti^{4+} site as an isovalent dopant, it shifts the Curie point of the

***Corresponding author: Mohammad Jellur Rahman,** Department of Physics, Bangladesh University of Engineering and Technology, Dhaka-1000, Bangladesh, e-mail: mjrahman@phy.buet.ac.bd
Myeesha Mostafa: Department of Physics, University of Dhaka, Dhaka-1000, Bangladesh; and Department of Physics, Jagannath University, Dhaka-1100, Bangladesh
Shamima Choudhury: Department of Physics, University of Dhaka, Dhaka-1000, Bangladesh

ceramics and depresses the dielectric peak [3]. Mn addition can also increase the average grain size of $BaTiO_3$, which reduces the AC resistivity.

By adopting the doping process, the electrical properties of the $BaTiO_3$ ceramics can be controlled. As Ce and Mn both have a significant role as a dopant on the properties of $BaTiO_3$, the effect of Ce and Mn co-doping on the various properties of $BaTiO_3$ was studied in this research.

2 Materials and methods

Ceramic samples with the general formula $Ba_{1-x}Ce_xTi_{1-y}Mn_yO_3$ (x, y = 0.00, 0.00; 0.01, 0.00; 0.02, 0.00; 0.03, 0.00; 0.00, 0.01; 0.00, 0.02; 0.00, 0.03; 0.01, 0.01; 0.02, 0.02; 0.03, 0.03) were prepared using the conventional solid state reaction technique. The raw BaO, CeO_2, TiO_2, and MnO_2 powders (Merck, Darmstadt, Germany, purity 98%) were screened and weighed appropriately, mixed and ground in an agate mortar for 15 min. Then the powders were wet mixed for 6 h using ball milling with the aid of zirconium balls having a diameter of 1 cm to form a homogeneous mixture. These mixtures were then dried and ground for 1.5 h. The samples were then calcined at 973 K for 2 h (with heating and cooling rate of 10 K/min) in a Nabertherm furnace (model HT 16/18, Bremen, Germany). The powders were again ground for 15 min and added with binder (81% C, 13.5% H, 2.9% O, and 2.6% N). Finally, these powders were pressed into pellets of thickness 2 mm and diameter 15 mm using a uniaxial hydraulic press (model HERZOG HTP 40, series no- MA 14822-1-1, Ennepetal, Germany) with a 40-kton force and sintered at 1473 K for 4 h with a heating and cooling rate of 10 K/min. The sintered pellets were polished and used for the measurement of the structural, morphological, and electrical properties. The surface morphology and average grain size of the samples

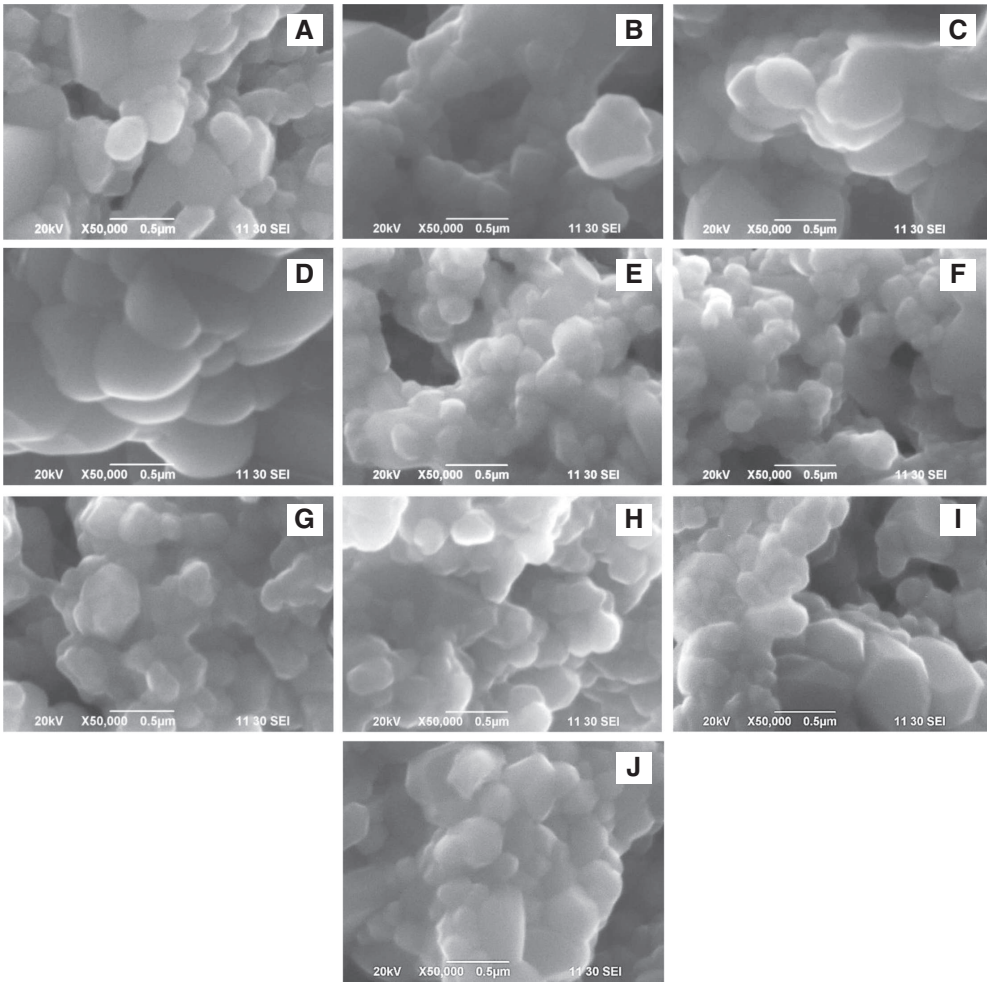

Figure 1: SEM images of the $Ba_{1-x}Ce_xMn_yTi_{1-y}O_3$ for x, y = (A) 0.00, 0.00, (B) 0.01, 0.00, (C) 0.02, 0.00, (D) 0.03, 0.0, (E) 0.00, 0.01, (F) 0.00, 0.02, (G) 0.00, 0.03, (H) 0.01, 0.01, (I) 0.02, 0.02, and (J) 0.03, 0.03.

were estimated by a scanning electron microscope (SEM, Hitachi S-3400N, Tokyo, Japan), and the structural property was investigated by an X-ray diffractometer (model Rigaku Ultima IV, Tokyo, Japan). For electrical measurements, high-conducting silver paste was applied on both sides of the pellets, and a Wayne Kerr 6500B series Precision Impedance Analyzer (Bognor Regis, West Sussex, UK) was used to measure the dielectric properties.

3 Results and discussion

SEM micrographs of the doped and co-doped $BaTiO_3$ samples with various concentrations of Ce and Mn are presented in Figure 1A–J, where the microstructures are observed to consist of intergranular pores and grains of various sizes and irregular shapes. The grain size is measured from the SEM micrographs. For each sample, several

Table 1: Values of average grain size, lattice parameter, and exponent, n, in $J \propto V^n$ and dielectric constant of the samples for different compositions.

Sample composition	Average grain size (μm)	Lattice parameter, a (Å)	Exponent, n, of the $J-V$ curve	Dielectric constant (ε_r)
$BaTiO_3$	0.230	4.0007	1.054	515
$Ba_{0.99}Ce_{0.01}TiO_3$	0.242	4.0006	0.900	1051
$Ba_{0.98}Ce_{0.02}TiO_3$	0.290	4.0004	1.340	219
$Ba_{0.97}Ce_{0.03}TiO_3$	0.580	3.9991	1.330	2800
$BaTi_{0.99}Mn_{0.01}O_3$	0.244	4.0028	1.190	623
$BaTi_{0.98}Mn_{0.02}O_3$	0.252	4.0027	0.945	1146
$BaTi_{0.97}Mn_{0.03}O_3$	0.265	4.0031	1.200	983
$Ba_{0.99}Ce_{0.01}Ti_{0.99}Mn_{0.01}O_3$	0.286	4.0005	1.380	837
$Ba_{0.98}Ce_{0.02}Ti_{0.98}Mn_{0.02}O_3$	0.291	4.0012	1.167	866
$Ba_{0.97}Ce_{0.03}Ti_{0.97}Mn_{0.03}O_3$	0.312	3.7664	1.312	968

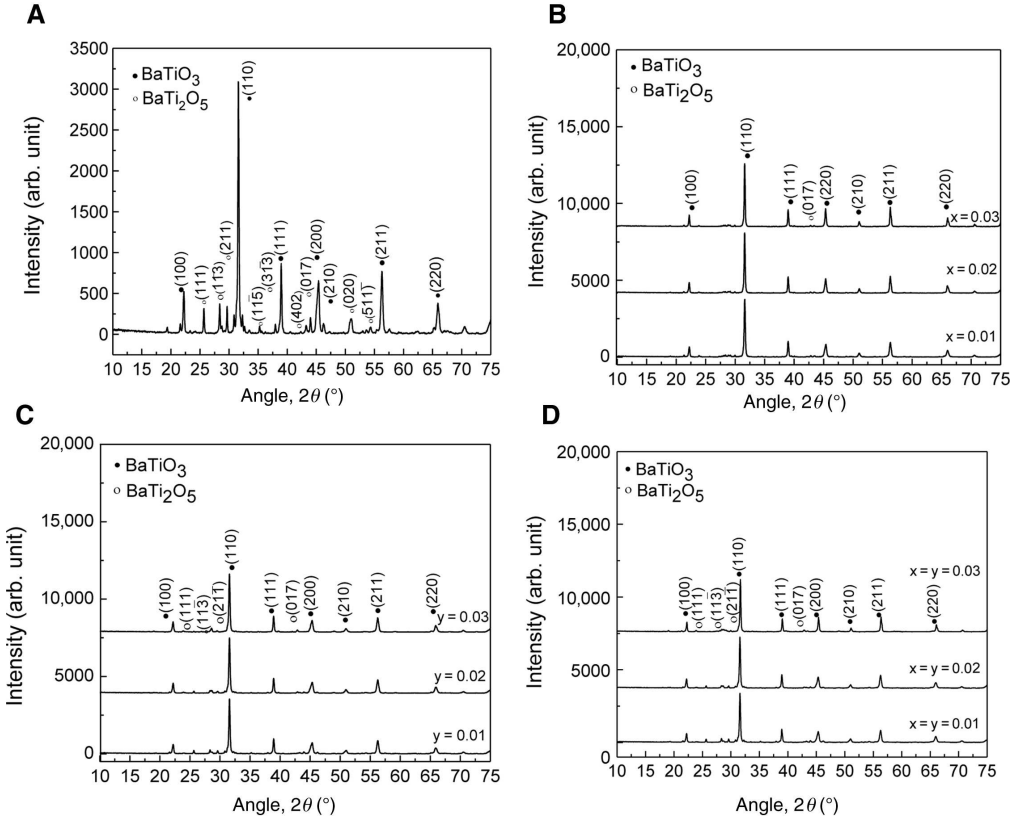

Figure 2: XRD pattern for the (A) pure, (B) Ce doped, (C) Mn doped, and (D) Ce-Mn-co-doped $BaTiO_3$, where the filled and unfilled circle represents the $BaTiO_3$ and $BaTi_2O_5$ phase, respectively.

SEM micrographs were taken to estimate the average grain size from at least 100 grains. The average grain size and lattice parameter for the different samples are presented in Table 1. It is observed that Ce doping has a significant role on the increase of grain size of the ceramics, and the grain size is the highest for 3 wt% of Ce doping (0.580 μm). However, no such sharp increase in grain size is observed for Mn doping, and therefore, it can be predicted that Mn doping cannot influence the microstructure as significantly as Ce. The increase or decrease in grain size mainly depends on the ionic radii of the substituting and parent atoms. The grain size increases if the ionic radius of the doped atom is larger than that of the parent atom and vice versa. Now in $BaTiO_3$, the Ba^{2+} site is considered as the A site and the Ti^{4+} site as the B site. Ce can occupy any of the sites due to its multi-valence. If Ce occupies the A site, due to having smaller ionic radius compared to Ba^{2+}, the grain size will decrease. However, in our case, the grain size is observed to increase, which is considered to happen due to the incorporation of Ce at the B site. Dependence of grain size distribution on a different site occupancy was described in many studies [12–15]. In a previous study, it was shown that Ce is most probably incorporated as 4+ on the B site and 3+ on the A site, and in $BaTiO_3$ with a Ti-rich phase, Ce^{3+} is incorporated in the A site ion, but in the Ba-rich case, it is incorporated in the B-site ion with either 3+ or 4+ valence [12]. Therefore, it can be considered that in our case, Ce is incorporated as 4+ at the Ti^{4+} sites rather than at the Ba^{2+} sites. As Ce has a larger ionic radius compared to that of Ti^{4+}, the grain size become larger due to the B-site occupancy. Owing to a similar reason, the increase in grain size is also observed for the co-doped sample with the increase of doping concentration.

The XRD patterns of all the compositions of pure, doped, and co-doped $BaTiO_3$ are shown in Figure 2, indicating the cubic phase of the ceramics. The absence of splitting of the XRD peaks confirms the cubic phase of $BaTiO_3$ with a small amount of secondary phase of $BaTi_2O_5$, which may be due to the use of raw BaO, CeO_2, MnO_2, and TiO_2 during the sample preparation [2, 16, 17]. It is also observed that some secondary phases of $BaCO_3$ exist [18], which may be due to the CO_2 in air. However, the

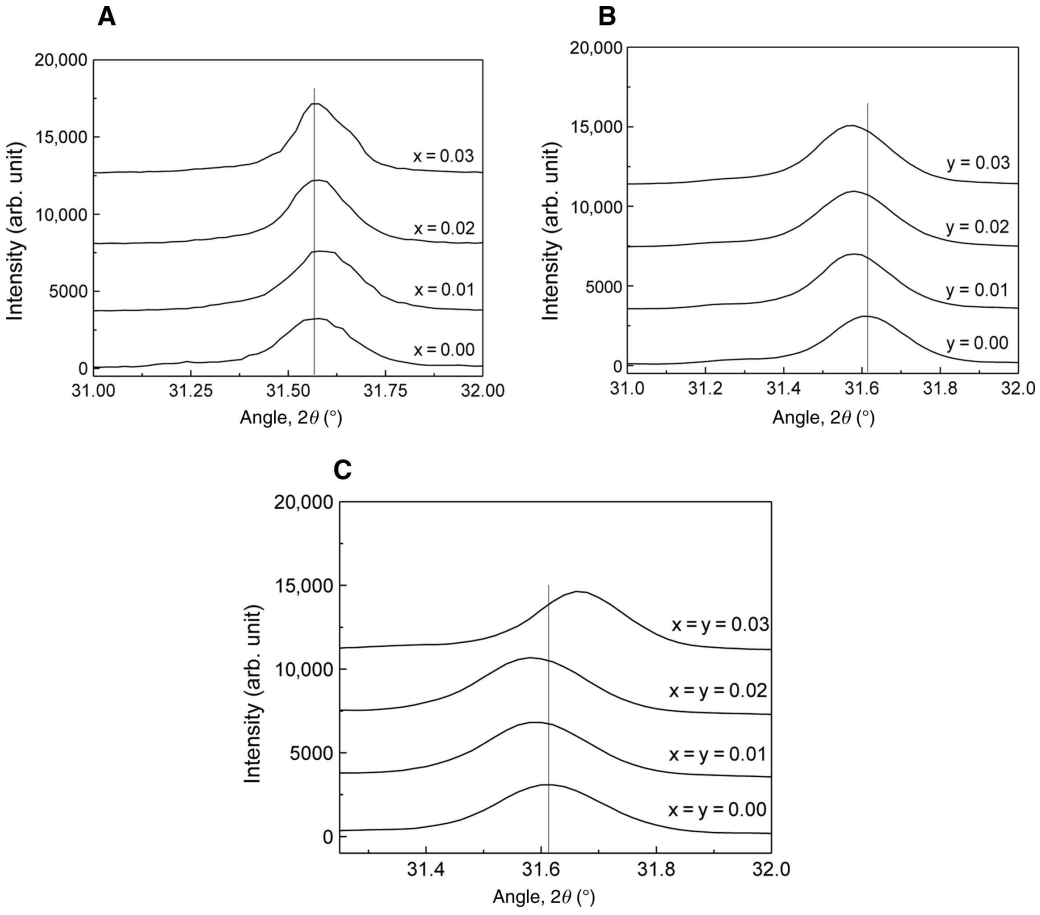

Figure 3: XRD profile around (110) peaks of the (A) $Ba_{1-x}Ce_xTiO_3$ (where x = 0.00, 0.01, 0.02, 0.03), (B) $BaMn_yTi_{1-y}O_3$ (where y = 0.00, 0.01, 0.02, 0.03), and (C) $Ba_{1-x}Ce_xMn_yTi_{1-y}O_3$ (where x = y = 0.00, 0.01, 0.02, 0.03) samples.

number of peaks of the $BaTi_2O_5$ phase decreases with the increase in concentration of the additives. The intensity of the major peak increases for the samples with Ce and Mn doping except for the samples having secondary $BaTi_2O_5$ phase, which indicates a better crystallization of the samples. No significant shifts in the XRD peaks are observed for the samples indicating that the structure of the samples remained almost unchanged.

Figure 3A–C shows shifting of the major peak (110) with the increase in the concentration of Ce and Mn, which is related to *d*-spacing, i.e. the lattice parameter, *a*, which is determined by the Nelson-Riley function $F(\theta)$ using the equation,

$$F(\theta) = \frac{1}{2}\left(\frac{\cos^2\theta}{\sin\theta} + \frac{\cos^2\theta}{\theta}\right) \quad (1)$$

The values of the lattice parameters are listed in Table 1. It is observed that the peaks shift to the right (toward the larger angle) for the Ce-doped $BaTiO_3$ samples and the lattice parameter decreases with the increase in Ce concentration in $BaTiO_3$, which may be due to the ionic radius of dopant Ce^{3+} (0.102 nm) being smaller than that of Ba^{2+} (0.135 nm) [19]. On the other hand, though the ionic radius of Mn^{4+} (0.064 nm) is smaller than that of Ti^{4+} (0.0745 nm), the peaks shift to the left instead of to the right, and the lattice parameter varies irregularly with the Mn concentration. This may be owing to the tendency of Mn to change its valence, where Mn^{2+} has ionic radii of 0.081 nm (lower spin) and 0.097 nm (higher spin), and Mn^{3+} has 0.072 nm (lower spin) and 0.0785 nm (higher spin) [11]. For the co-doped $BaTiO_3$, the irregular value of the lattice parameter is also due to this tendency to change the valence of Mn.

The energy-dispersive X-ray (EDX) detector was used for the elemental analysis of the samples, and the relative counts of X-ray versus energy spectrum is obtained. The representative curve as shown in Figure 4 indicates the Ce- and Mn-rich regions, which can be synchronized with the perovskite phase in the $Ba_{1-x}Ce_xTi_{1-y}Mn_yO_3$ with $x = y = 0.02$ sample. The EDX analysis also indicates that there is no impurity element in the sample.

The room temperature $J-V$ characteristic curves of all the samples are shown in Figure 5A–C, which indicate that the current density increases almost linearly with the applied voltage, i.e. the samples show nearly an ohmic nature, which is predicted from the calculated values of the exponent n, in the $J \propto V^n$ equation that lies between 0.9 and 1.38 [2]. The values of n of the $J-V$ curves are given in Table 1.

To understand the effect of Ce and Mn doping on the electrical property of the $BaTiO_3$, the frequency-dependent

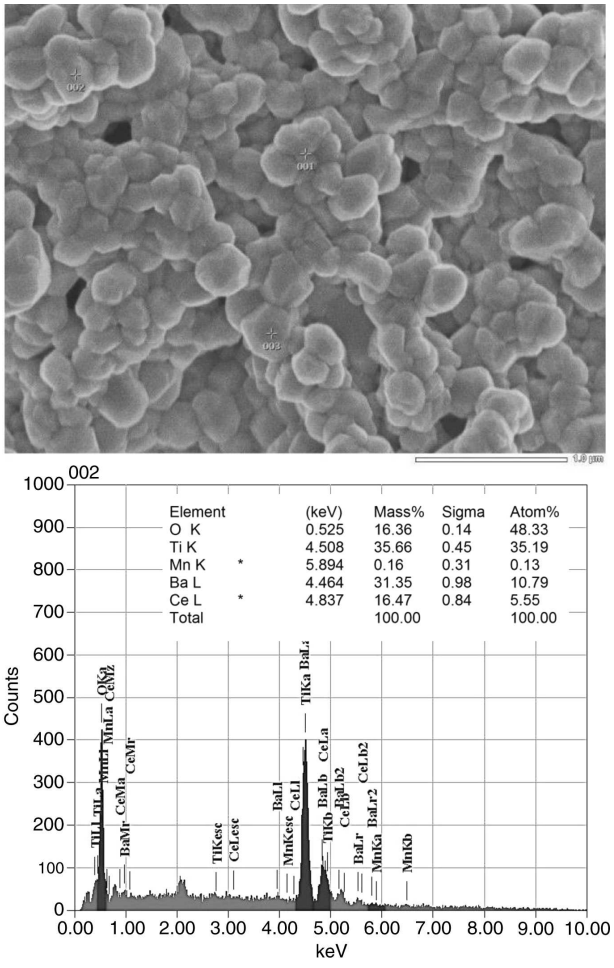

Figure 4: SEM and EDX spectrum of the $Ba_{1-x}Ce_xTi_{1-y}Mn_yO_3$ ($x = y = 0.02$) sample and the elemental data.

AC resistivity of the samples was analyzed. Figure 6A shows the variation of resistivity with frequency of the different compositions of $BaTiO_3$, where it is observed that in the lower-frequency region (up to 100 kHz), resistivity drops sharply as the frequency increases, but at the higher-frequency region, it becomes independent of frequency. Figure 6B shows the variation of resistivity with the concentration of dopants. The resistivity of the samples is observed to decrease in all cases with the concentration of doping. As a consequence of strong dependence of resistivity on the grain size of the $BaTiO_3$, it can be conjectured that with the increase in grain size, resistivity decreases. The decreases in resistivity with the increase in Ce doping may be due to the better compaction of the samples. Furthermore, a partial exchange between the Ba^{2+} and Ce^{3+} sites may cause the increase in carrier concentration, and therefore, resistivity decreases [2]. Similar results are also observed for the Mn-doped $BaTiO_3$ and Ce, Mn-co-doped $BaTiO_3$ samples.

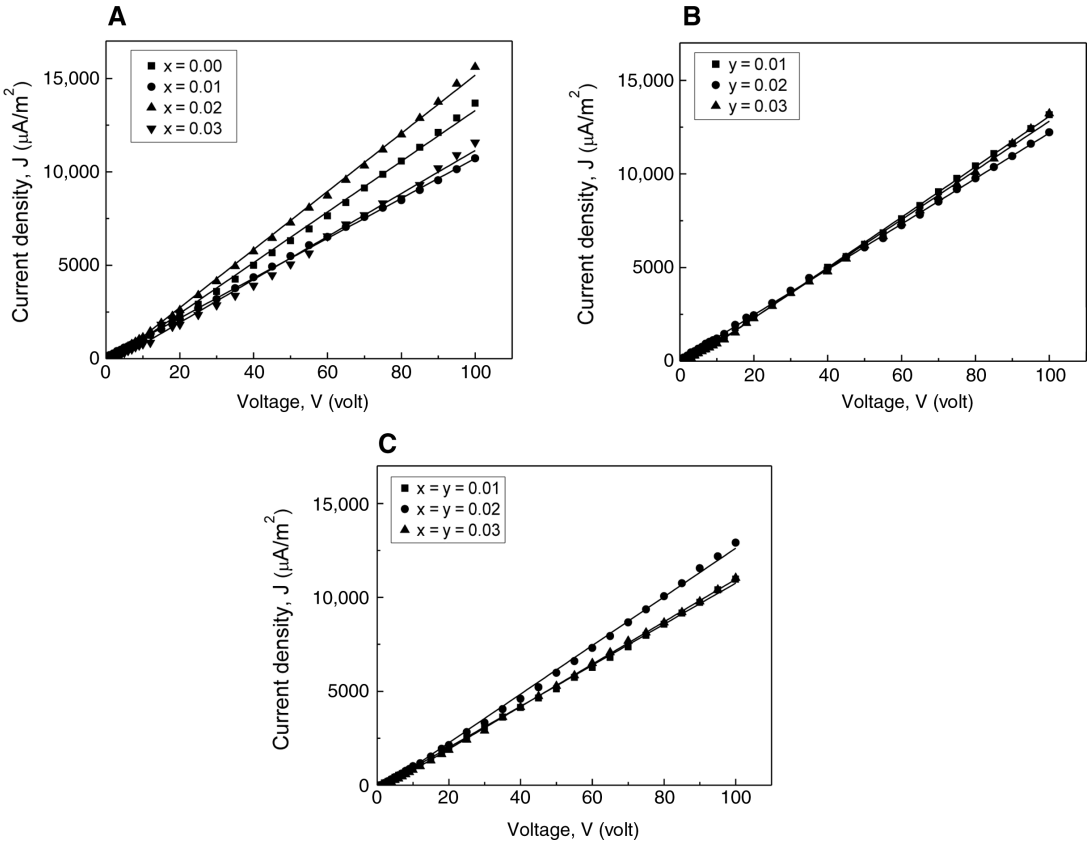

Figure 5: DC electrical properties of the (A) $Ba_{1-x}Ce_xTiO_3$ (x = 0.0, 0.01, 0.02, 0.03), (B) $BaTi_{1-y}Mn_yO_3$ (y = 0.01, 0.02, 0.03), (C) $Ba_{1-x}Ce_xTi_{1-y}Mn_yO_3$ (x = 0.01, y = 0.01; x = 0.02, y = 0.02; x = 0.03, y = 0.03) samples.

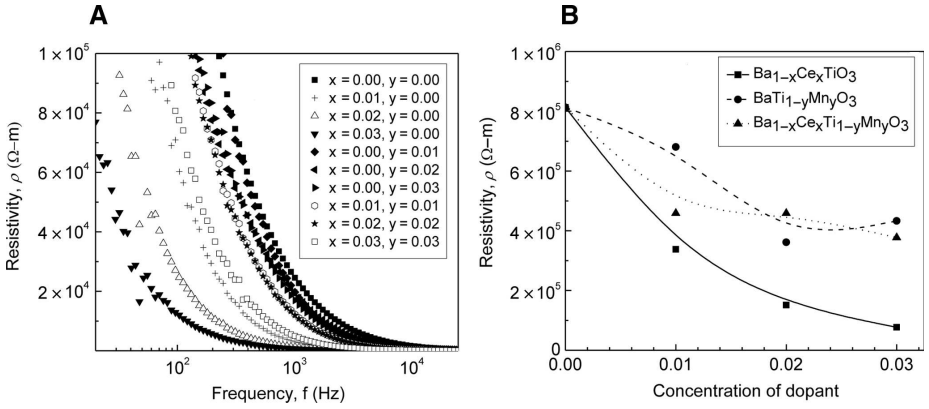

Figure 6: Plot of the (A) resistivity versus frequency and (B) resistivity versus concentration of additive curves of all the samples at room temperature.

It is observed from Figure 7A that at a very low frequency (below 1 kHz), the value of the dielectric constant ε_r decreases with increasing frequency [2, 20–23], which suggests that the presence of more than one kind of polarization (i.e. interfacial, atomic, dipolar, electronic, etc.) is effective in the samples. However, beyond 1.5 kHz, ε_r becomes almost constant with frequency. At a higher-frequency region, it may be conjectured that mainly atomic and electronic polarization contributes to ε_r [24]. Again, the value of ε_r increases with the increase in the doping concentration in $BaTiO_3$. The result given in Table 1 shows that the addition of Mn causes a slight increase

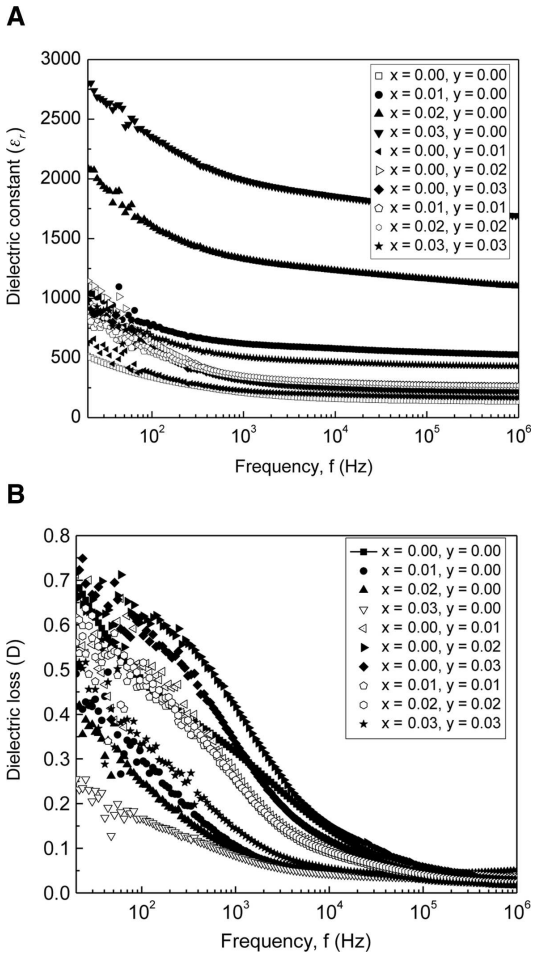

Figure 7: Variation of the (A) dielectric constant and (B) dielectric loss as a function of frequency.

in ε_r, and a further increase occurs due to Mn and Ce co-doping. However, $BaTiO_3$ doped with 3 wt% Ce shows the highest ε_r value. As the lattice parameter decreases with doping and co-doping, there may be an increase in density of the samples [2]. Again, the increase in density increases the dielectric constant [25]. So the increase in the dielectric constant of the doped and co-doped $BaTiO_3$ could be happened due to the increase in the density with doping.

The variation of the dielectric loss D with frequency for the different compositions of the samples is shown in Figure 7B, where the D value drops gradually in the lower-frequency region (up to 4 kHz) and, then, remains almost constant at the higher-frequency region. However, at a higher-frequency range, the value of D decreases slightly with the increase in frequency. In the case of the Ce-doped $BaTiO_3$, the value of D decreases as the doping concentration increases [2]. For the Mn-doped $BaTiO_3$, the D value varies irregularly with the increase in the concentration of the dopant.

4 Conclusions

The grains of the $Ba_{1-x}Ce_xTi_{1-y}Mn_yO_3$ samples are observed to be of irregular shape. Although Ce doping has a significant effect on the increase in grain size of the ceramics, no such sharp increase in grain size is observed for Mn doping. The XRD pattern confirmed the single-phase structure of the samples having a very small amount of impurity phases, which reduces due to the addition of Ce and Mn in $BaTiO_3$. All the samples show nearly an ohmic nature with very low conductivity. The AC resistivity, dielectric constant, and dielectric loss of the samples decrease in the low-frequency region, but the AC resistivity and the dielectric constant became nearly constant above 100 kHz and above 1 kHz, respectively. The value of the resistivity decreases and the dielectric constant increases with Ce and Mn concentration. Besides, the dielectric loss is observed to decrease with the increase in the concentration of the Ce dopant, but the variation becomes irregular when Mn is doped. $BaTiO_3$ doped with Mn showed an improved property than that of pure $BaTiO_3$, but further improvement can be achieved by co-doping with Ce. Although a better result can be obtained from the Ce-doped $BaTiO_3$, to reduce the production cost, it would be convenient to co-dope $BaTiO_3$ with Ce and Mn.

Acknowledgments: The authors acknowledge the laboratory facilities of Nano and Advanced Materials Lab, Department of Physics, University of Dhaka; Department of Physics, Bangladesh University of Engineering and Technology (BUET); Department of Glass and Ceramic Engineering, BUET; and the Centre for Advance Research in Science (CARS), University of Dhaka.

References

[1] Vijatovic MM, Bobic JD, Stojanovc BD. *Sci. Sinter.* 2008, 40, 155–165.
[2] Yasmin S, Choudhury S, Hakim MA, Bhuiyan AH, Rahman MJ. *J. Ceram. Process. Res.* 2011, 12, 387–391.
[3] Islam R, Choudhury S, Bhuyan AH, Rahman SN, Rahman MJ. *J. Ceram. Process. Res.* 2012, 13, 248–251.
[4] Choudhury S, Akter S, Rahman MJ, Bhuyan AH, Rahman SN, Khatun N, Hossain MT. *J. Bangladesh Acad. Sci.* 2008, 32, 221–229.
[5] Khan M. *J. Am. Ceram. Soc.* 1971, 54, 452–454.
[6] Rahman MN, Manalert R. *J. Eur. Ceram. Soc.* 1998, 18, 1063–1071.
[7] Stojanovic BD. In *Proc. Ninth World Round Table Conference on Sintering*, Stojanovic, BD, Skorokhod, VV, Nikolic, MV, Eds., Kluwer Academic/Plenum Publishers: New York, 1999, pp 367–376.

[8] Alart G, Hennings D, Dewith G. *J. Appl. Phys.* 1985, 58, 1619–1625.
[9] Hwang JH, Han YH. *J. Am. Ceram. Soc.* 2001, 84, 1750–1754.
[10] Rahman MJ, Choudhury S, Bhuiyan AH, Rahman SN, Khan AH. *J. Bangladesh Acad. Sci.* 2007, 31, 137–141.
[11] Vijatovic Petrovic MM, Bobic JD, Grigalaitis R, Stojanovic BD, Banys J. *Acta. Phys. Polonica A* 2013, 124, 155–160.
[12] Tsur Y, Dunbar TD, Randall CA. *J. Electroceram.* 2001, 7, 25–34.
[13] Park JG, Oh TS, Kim YH. *J. Mater. Sci.* 1992, 27, 5713–5719.
[14] Pu Y, Chen W, Chen S, Langhammer HT. *Cerâmica* 2005, 51, 214–218.
[15] Maikhuri N, Panwar AK, Jha AK. *J. Appl. Phys.* 2013, 113, 17D915.
[16] Mahbub R, Hossain MS, Islam MF. *Matter. Sci.* 2013, 20, 45–53.
[17] Deng Z, Dai Y, Chen W. *Nanoscale Res. Lett.* 2010, 5, 1217–1221.
[18] Jamal A, Naeem M, Iqnal Y. *J. Pak. Mater. Soc.* 2008, 2, 91–95.
[19] Kotlyarchuk A, Klymenko V, Dubovitskaya N, Lobunets T, Shatskikh S, Ragulya A. *Proceeding of the International Conference Nanomaterials: Applications and Properties*, Alushta, the Crimea, Ukraine, 2012, 1, 04NMEEE04(1-3).
[20] Sen S, Choudhury RNP. *J. Mater. Sci.* 2005, 40, 5457–5462.
[21] Paunovic V, Zivkovic L, Vracar L, Mitic V, Miljkovic M. *Serbian J. Electrical Eng.* 2004, 1, 89–98.
[22] Sarah P, Surayanarayana SV. *Bull. Mater. Sci.* 2003, 26, 745–747.
[23] Paunovic V, Mitic V, Pavlovic V, Miljkovic M, Zivkovic L. *Sci. Sinter.* 2012, 44, 223–233.
[24] Panigrahi A, Singh NK, Choudhary RPN. *J. Phys. Sol.* 2002, 63, 213–219.
[25] Lanza VL, Herrmenn DB. *J. Polym. Sci.* 1958, 28, 622–625.